Electronic Supplementary Material (ESI) for ChemComm.

Supporting Information

Two-step spin crossover by guest-disorder induced local symmetry breaking within a 3D Hofmann-like framework

Hunter J. Windsor,[a] William Lewis,[a,b] Suzanne M. Neville,[c] Samuel G. Duyker,[a,b] Deanna M. D'Alessandro[a] and Cameron J. Kepert*[a]

[a]School of Chemistry, The University of Sydney, Sydney, NSW 2006, Australia.
Email: cameron.kepert@sydney.edu.au

[b]Sydney Analytical, The University of Sydney, Sydney, New South Wales, 2006, Australia

[c]School of Chemistry, University of New South Wales, Sydney, NSW, 2052, Australia

Contents

S1 – Synthesis

S2 – Single Crystal X-Ray Diffraction

S3 – Powder X-Ray Diffraction

S4 – Magnetic Susceptibility

S5 – Raman Spectroscopy

S6 – Thermogravimetric Analysis

S7 – UV-Visible Spectroscopy

S8 – Density Functional Theory

S9 – References

S1 – Synthesis

General

All reagents and solvents were purchased from Sigma Aldrich, Merck, or A.K. Scientific and were used without further purification unless otherwise stated. *Caution!* Iron(II) perchlorate hydrate is potentially explosive and should therefore be handled with care and in small amounts.

Synthesis of 4,7-di(4-pyridyl)-2,1,3-benzothiadiazole (dpbtz)

Dpbtz was synthesised by a Suzuki-Miyaura coupling *via* modification of a previously reported method which employed a Stille coupling.[1] To an argon degassed mixture of 1,4-dioxane (30 mL) and distilled water (10 mL) was added 4,7-dibromo-2,1,3-benzothiadiazole (1.18 g, 4.01 mmol), 4-pyridineboronic acid (1.05 g, 8.56 mmol), anhydrous potassium carbonate (1.80 g, 1.30 mmol), and tetrakis(triphenylphosphine)palladium(0) (250 mg, 0.216 mmol). The resulting mixture was heated at reflux for 18 h to produce an orange-gold solution. After being cooled to room temperature, the mixture was extracted into chloroform (3 × 150 mL), with intermediate washings with distilled water (3 × 100 mL). The combined organic extracts were dried with anhydrous magnesium sulfate and the solvent was removed under reduced pressure. The crude product was recrystallised from ethanol to furnish yellow needles of the title compound (640 mg, 2.20 mmol, 55%). **M.p.** 251–253 °C (lit.[1] 258–260 °C). **^{1}H NMR** (400 MHz, $CDCl_3$, ppm): δ 8.79 (d, $^{3}J_{H\text{-}H}$ = 6.04 Hz, 4H), 7.92 (d, $^{3}J_{H\text{-}H}$ = 6.04 Hz, 4H), 7.92 (s, 2H). **^{13}C NMR** (100 MHz, $CDCl_3$, ppm): δ 153.83, 150.61, 144.92, 132.30, 128.81, 123.90. **IR** (ATR, cm^{-1}): v 3039 (w), 1594 (m), 1409 (m), 1216 (m), 1071 (m), 994 (m), 887 (m), 816 (s), 713 (s), 624 (m), 547 (s). **UV-Vis** ($CHCl_3$, nm): λ_{max} 361, 319, 310, 274. **MS** (ESI, MeOH): m/z calculated for $C_{16}H_{10}N_4S$ $[M+H]^+$: 291.06, found: 291.04. **Elemental analysis** calculated for $C_{16}H_{10}N_4S$ (%): C 66.18, H 3.47, N 19.30, S 11.05; found (%) C 66.21, H 3.30, N 19.30, S 11.16.

Single crystal synthesis of $[Fe^{II}(dpbtz)(Au^{I}(CN)_2)_2]\cdot 0.5chry\cdot 1.5MeCN$ (Au ⊃ chry)

X-ray quality single crystals of **Au ⊃ chry** were synthesised by slow diffusion using the vial-in-vial method. To a flat bottomed 2 mL threadless vial was added dpbtz (2.85 mg, 0.00982 mmol), potassium dicyanoaurate(I) (5.65 mg, 0.0196 mmol), and chrysene (224 mg, 0.981 mmol). To a 21 mL scintillation vial was added iron(II) perchlorate hydrate (2.50 mg, 0.00981 mmol). The smaller vial was then placed within the larger vial and then both vials were carefully filled with the solvent ethanol:acetonitrile (1:1, *ca.* 20 mL). Yellow block crystals of **Au ⊃ chry** were produced after one week. **IR** (ATR, cm^{-1}): v 2170 (s), 1610 (s), 1549 (w), 1512 (w), 1481 (w), 1428 (m), 1226 (w), 1071 (w), 1018 (m), 817 (s), 765 (s), 725 (s), 625 (m), 556 (m), 522 (s), 475 (s). **UV-Vis** (nm): λ_{max} 472, 355, 318, 306, 267, 259, 239, 232. **Elemental analysis** calculated for $C_{20}H_{10}N_8SFeAu_2\cdot 0.5(C_{18}H_{12})$ (%): C 36.35, H 1.68, N 11.69, S 3.35; found (%) C 36.30, H 1.67, N 11.60, S 3.28.

* Elemental microanalysis of metal–organic frameworks can produce unreliable and highly variable results due to their inherent porosity and tendency to include

unmodellable solvent contributions. Single crystals of **Au** ⊃ **chry** were first evacuated to remove surface and pore included acetonitrile molecules. Before the elemental microanalysis experiment was performed, the crystals were additionally exposed to an in situ pre-drying procedure at 110 °C which resulted in quantitative removal of any remaining acetonitrile. The calculated formula for the elemental microanalysis experiment includes only the host framework and that of the half-occupied chrysene molecule which was not removed during the evacuation and drying procedures. The formula of the solvated material includes the contribution of 1.5 acetonitrile molecules, hence the discrepancy between the two formulae.

Fig. **S1** Illustrative example of a vial-in-vial diffusion, with red and blue coloured solutions for clarity. For **Au** ⊃ **chry** syntheses, the inner 2 mL vial contained a solution of potassium dicyanoaurate(I) and **dpbtz** in 50% acetonitrile in ethanol, while the outer 21 mL vial contained iron(II) perchlorate hydrate in the same solvent combination. Slow diffusion of the reagents through a carefully layered solution of 50% acetonitrile in ethanol led to the formation of single crystals over periods of days to weeks.

S2 – Single Crystal X-Ray Diffraction

Crystals of **Au** ⊃ **chry** were examined on an Agilent Technologies SuperNova Dual Source diffractometer equipped with a SuperNova microfocus source outputting mirror-monochromated Mo-Kα (λ = 0.71073 Å) radiation and fitted with an Atlas CCD detector, or on a Bruker APEX2 FR591 diffractometer equipped with an Incoatec IμS 2.5 source outputting mirror-monochromated Mo-Kα (λ = 0.71073 Å) radiation and fitted with a Bruker APEX-II CCD detector. Both diffractometers were equipped with an Oxford Cryosystems Cryostream 700 for temperature control. Due to the

experimental set up, different crystals were used for each temperature measurement. In both cases, yellow block crystals of **Au ⊃ chry** were isolated directly from the crystallisation mother liquor and then mounted onto a Hampton Research CrystalCap Spine HT CryoLoop utilising Paratone-N oil as a cryoprotectant. The crystals were then attached to the respective instrument goniometers and cooled to the desired temperature before data were collected. Reflection intensities were integrated from a sphere of data recorded in 1.0–1.5° increments about ϕ and ω rotations. Unit cell determination, data integration, frame scaling, and absorption corrections (multi-scan implemented in SADABS with beam profile correction, or Gaussian grid face-indexed numerical integration with beam profile correction) were performed in CrysAlisPro[2] (100 K and 250 K) or APEX2 (185 K).[3] Structure solutions were obtained by intrinsic phasing methods using SHELXT-2018/2[4] and were refined by a full-matrix least squares on all unique F^2 values using SHELXL-2018/3[5] within OLEX2-1.5.[6] For each temperature, all non-hydrogen atoms were refined with anisotropic thermal parameters unless otherwise stated (full details can be found in the _refine_special_details sections of each crystallographic information file (CIF)), with hydrogen atoms being added geometrically and refined using riding thermal parameters. Solvent accessible pore space was calculated via PLATON.[7] Structures (CCDC numbers: 2166788, 2166789, 2166790) have been deposited in the CCDC and are accessible free of charge via the internet.

The X-ray crystal structure of Au ⊃ chry

The chrysene guest molecule could be located from the Δ*F* map as a set of residual electron density peaks. The first step was to recognise that the first set of residual electron density peaks were related to another set of equivalent peaks by a crystallographic two-fold symmetry element, and accordingly to model a single set as a chrysene molecule, with each of the 18 carbons and 12 hydrogens in **PART -1** (to suppress bonds to symmetry equivalents) and with 50% occupancy. It became immediately apparent that multiple geometric and thermal restraints would be required to obtain a chemically reasonable molecule. All equivalent 1,2- and 1,3- carbon-carbon distances of the chrysene molecule were restrained to be approximately equal by applying **SADI** restraints, and an approximately flat geometry was achieved by applying the **FLAT** restraint. The thermal parameters of the chrysene were stable to an unrestrained anisotropic refinement, but nevertheless produced unphysical ADPs. Therefore, enhanced rigid bond **RIGU** and similarity **SIMU** restraints were applied across the entire molecule. This allowed the molecule to sensibly refine with anisotropic thermal parameters, except for C24 and C25, which still could not be refined anisotropically and were thus left isotropic. Presumably, this effect was due to the strong overlap of the C24 and C25 carbons and the acetonitrile molecule that was also present and half-occupied, which caused multiple refinement parameter correlations.

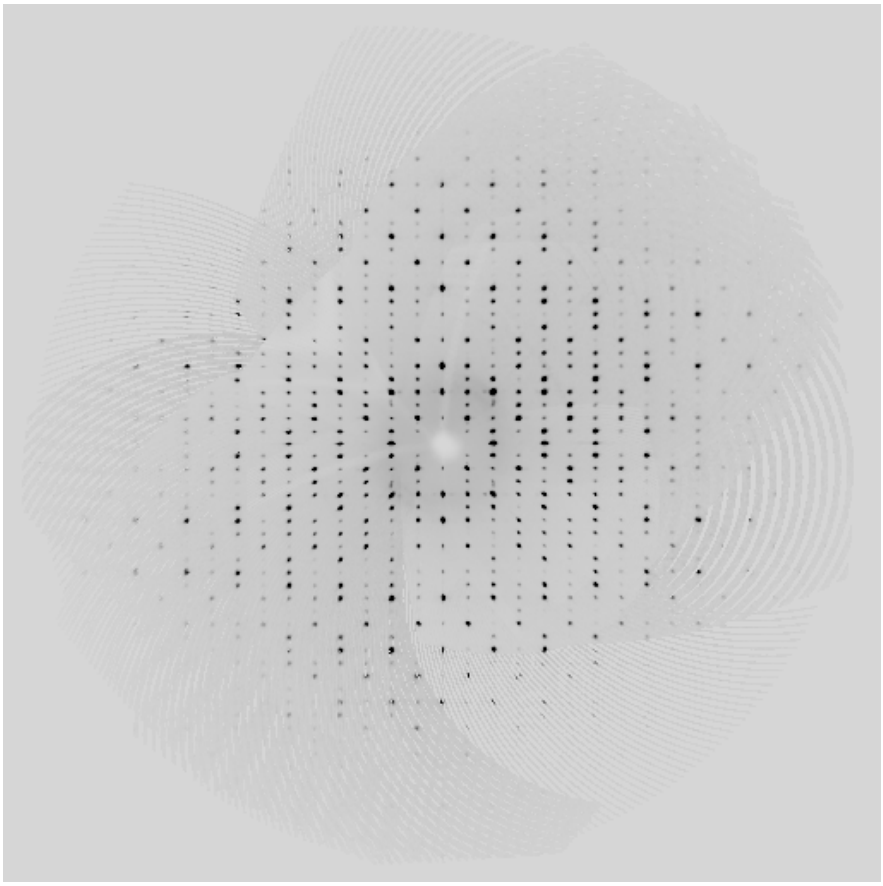

Fig. **S2.1** 0kl precession image at 185 K.

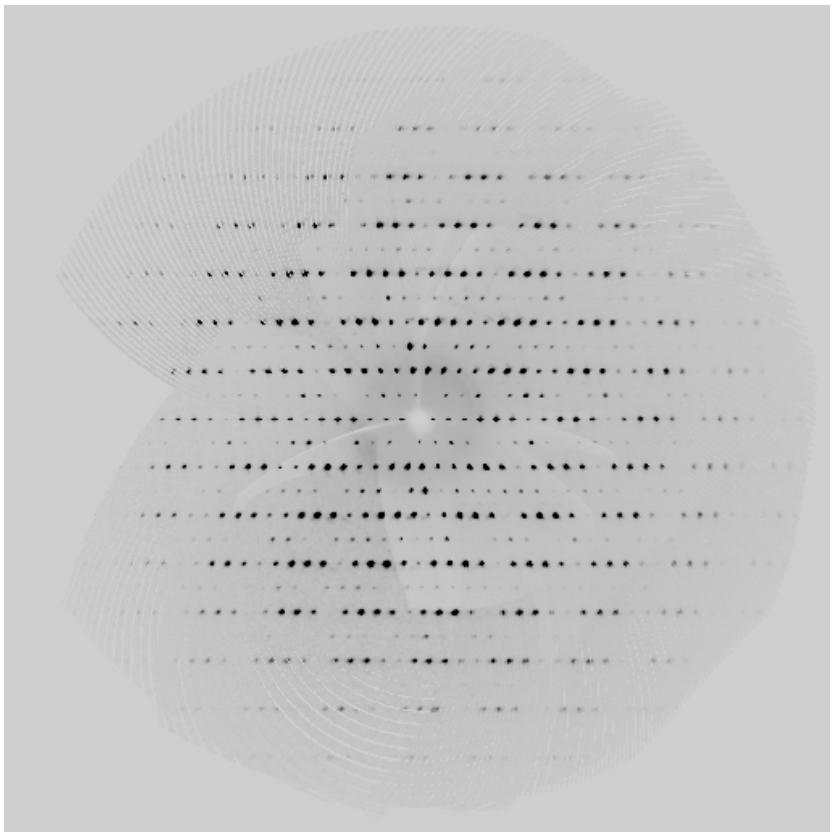

Fig. **S2.2** h0l precession image at 185 K.

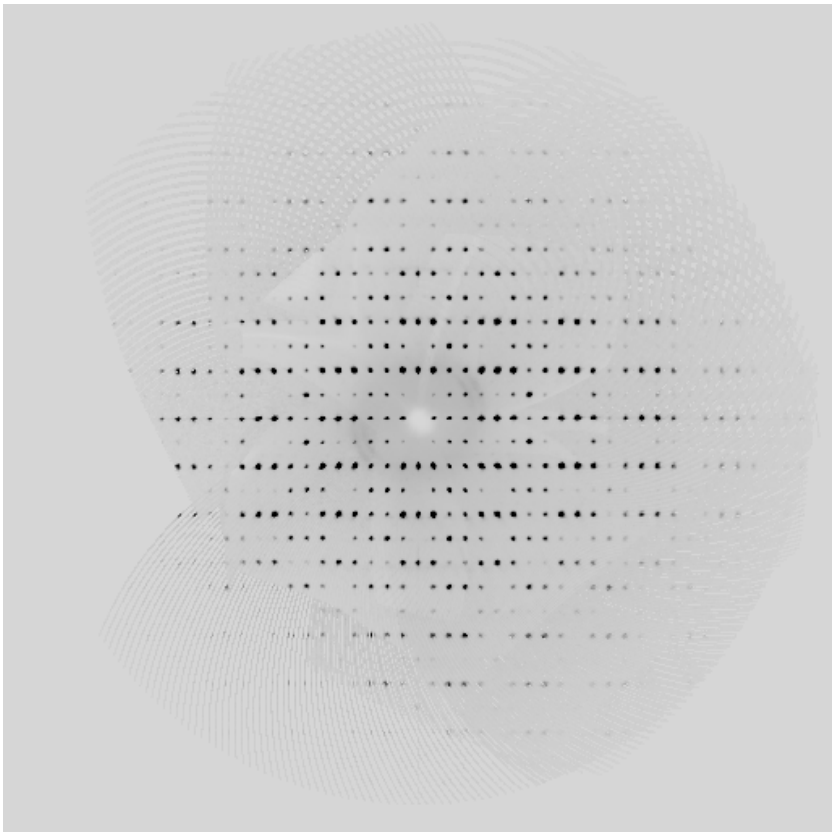

Fig. **S2.3** hk0 precession image at 185 K.

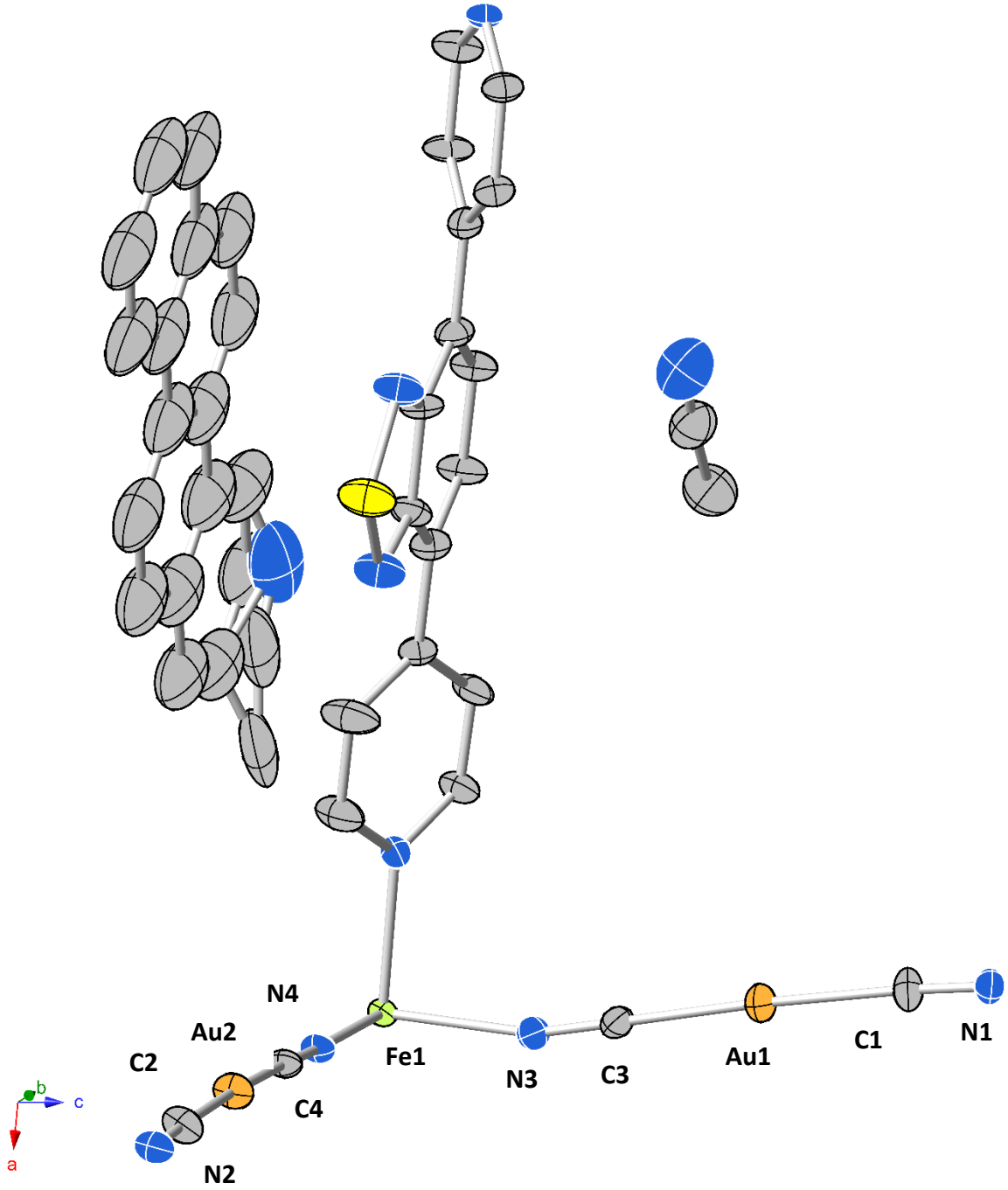

Fig. S2.4 Asymmetric unit of **Au ⊃ chry** at 250 K with thermal ellipsoids at 30% probability. Hydrogen atoms omitted for clarity. Atom colours: C (grey), N (blue), S (yellow), Fe (green), Au (gold).

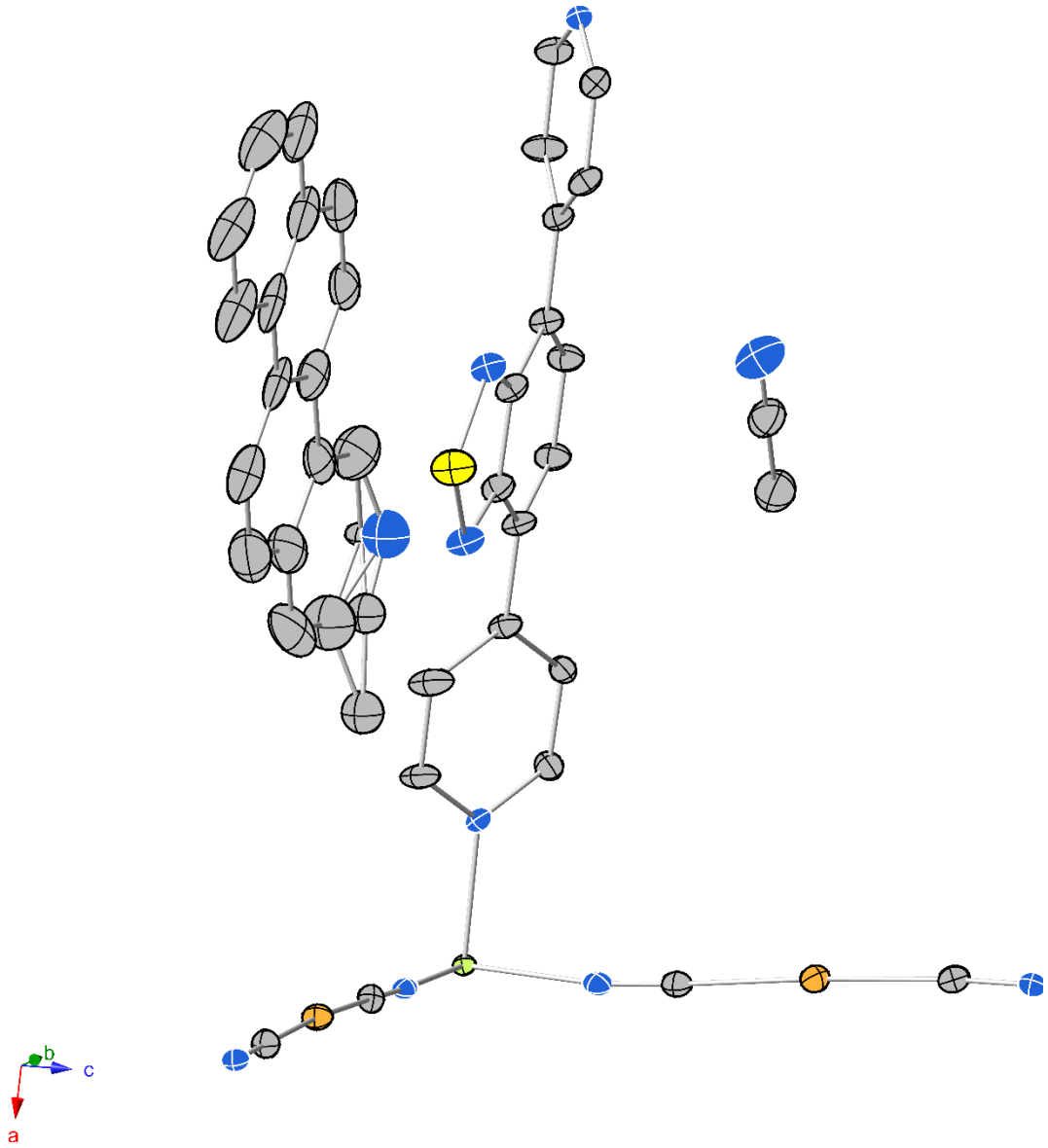

Fig. S2.5 Asymmetric unit of **Au** ⊃ **chry** at 185 K with thermal ellipsoids at 30% probability. Hydrogen atoms omitted for clarity. Atom colours: C (grey), N (blue), S (yellow), Fe (green), Au (gold).

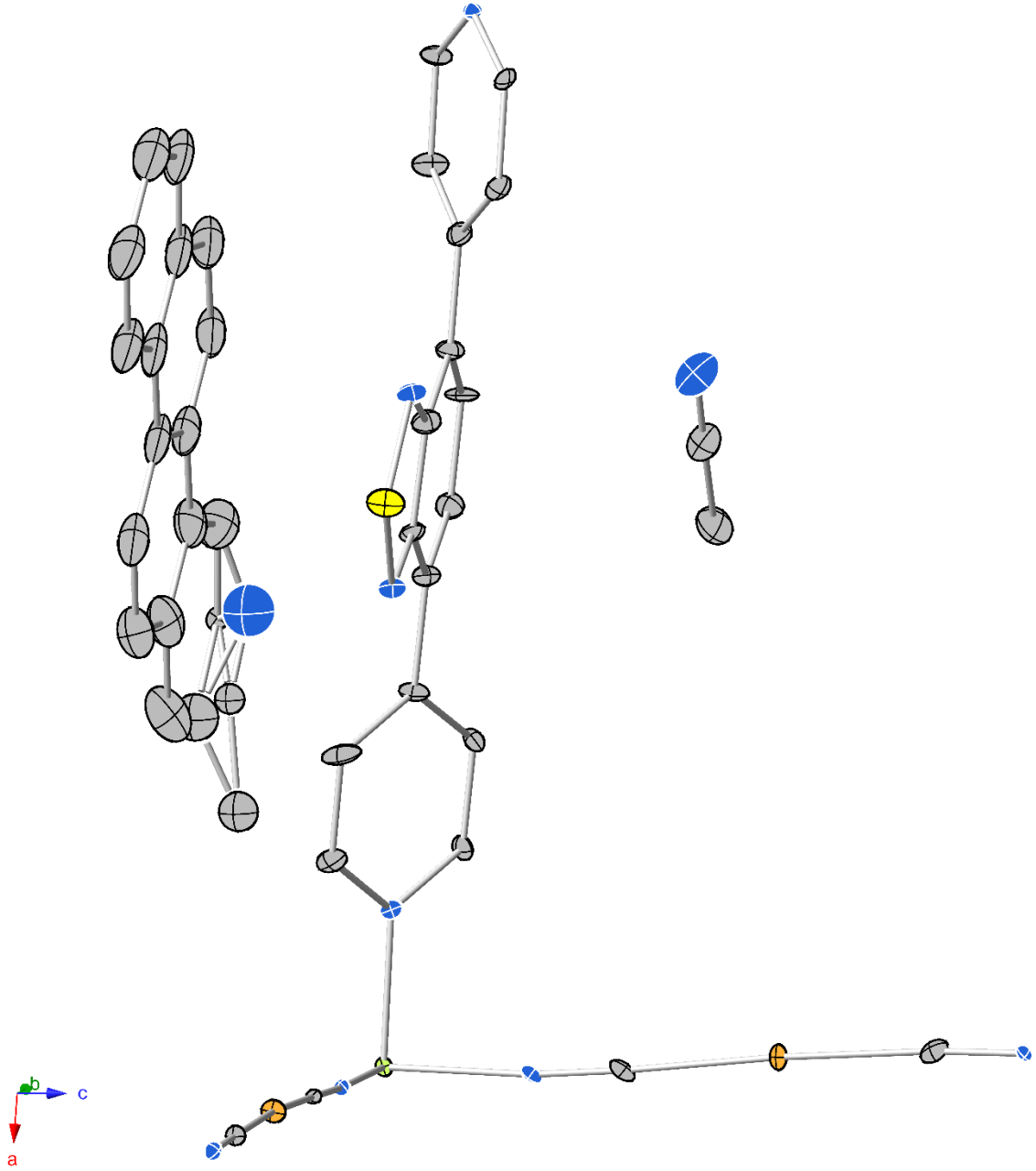

Fig. S2.6 Asymmetric unit of **Au ⊃ chry** at 100 K with thermal ellipsoids at 30% probability. Hydrogen atoms omitted for clarity. Atom colours: C (grey), N (blue), S (yellow), Fe (green), Au (gold).

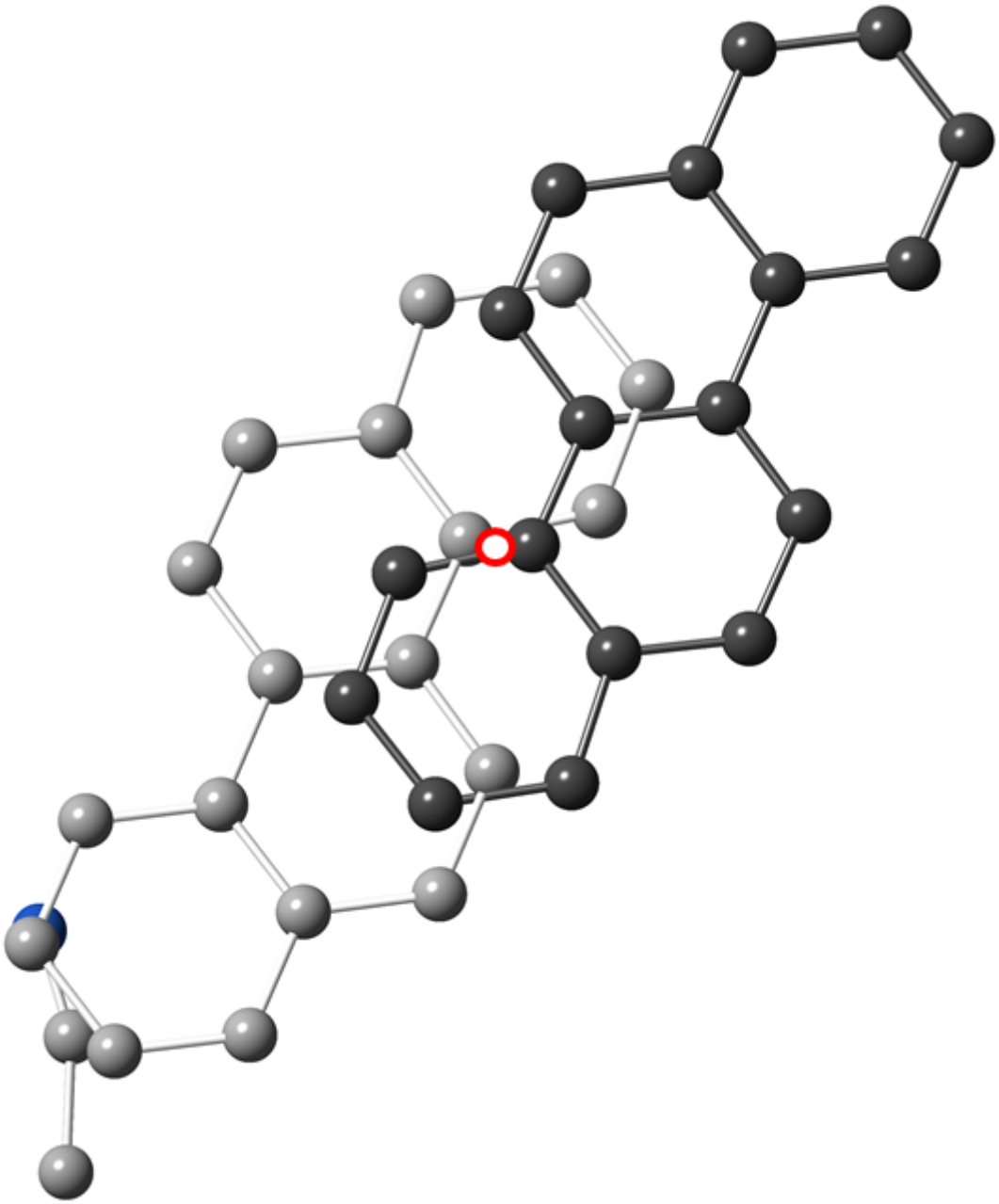

Fig. S2.7 Fragment of **Au** ⊃ **chry** at 250 K showing the chrysene guest molecule disordered across an inversion centre (○) and a superimposed half-occupied acetonitrile. Hydrogen atoms omitted for clarity.

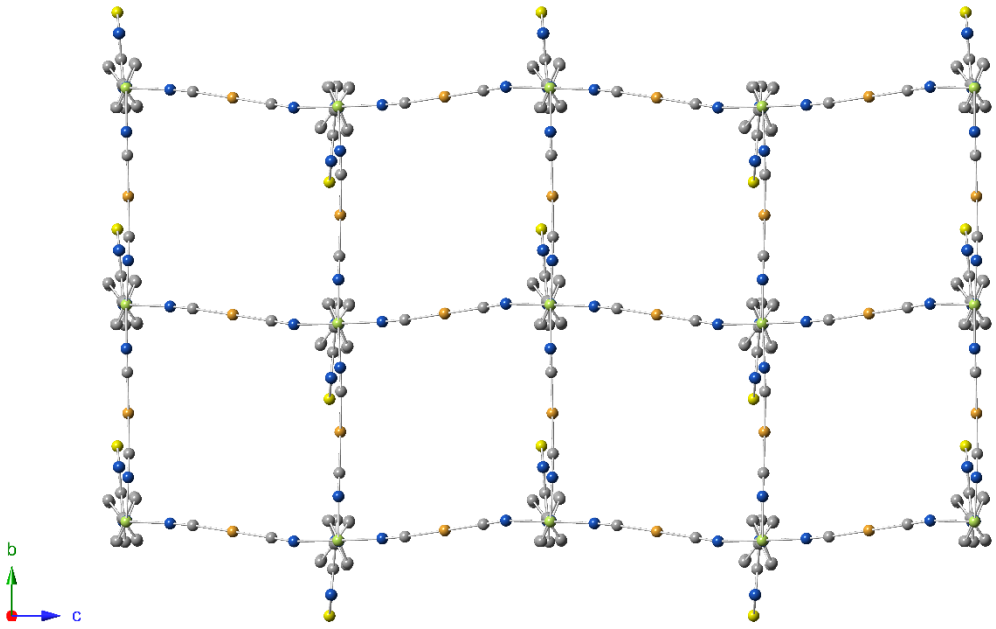

Fig. S2.8 Au ⊃ chry at 250 K viewed along the *a*-axis. Hydrogen atoms and guest molecules have been omitted for clarity. Atom colours: C (grey), N (blue), S (yellow), Fe (green), Au (gold).

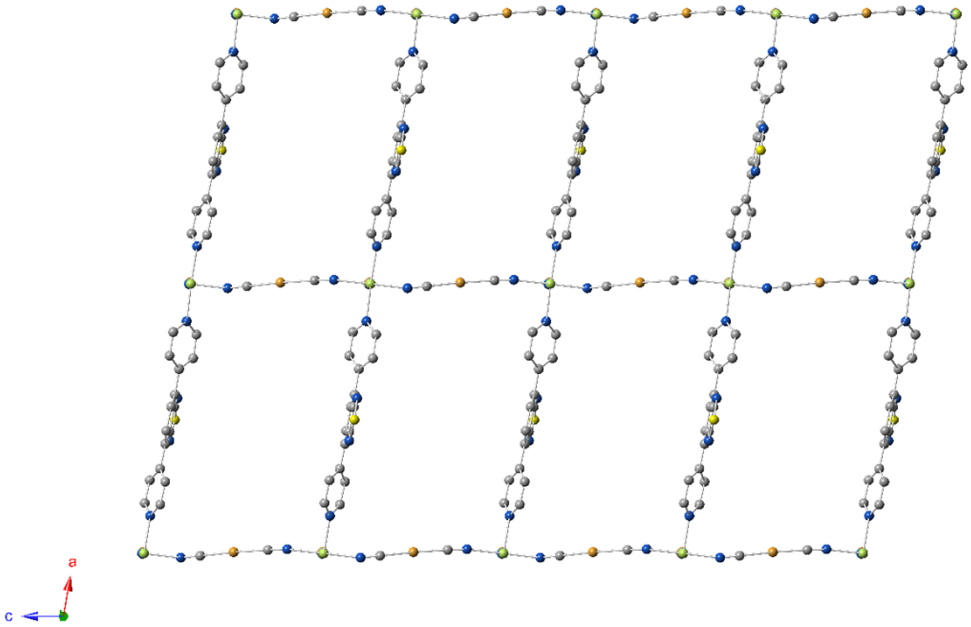

Fig. S2.9 Au ⊃ chry at 250 K viewed along the *b*-axis. Hydrogen atoms and guest molecules have been omitted for clarity. Atom colours: C (grey), N (blue), S (yellow), Fe (green), Au (gold).

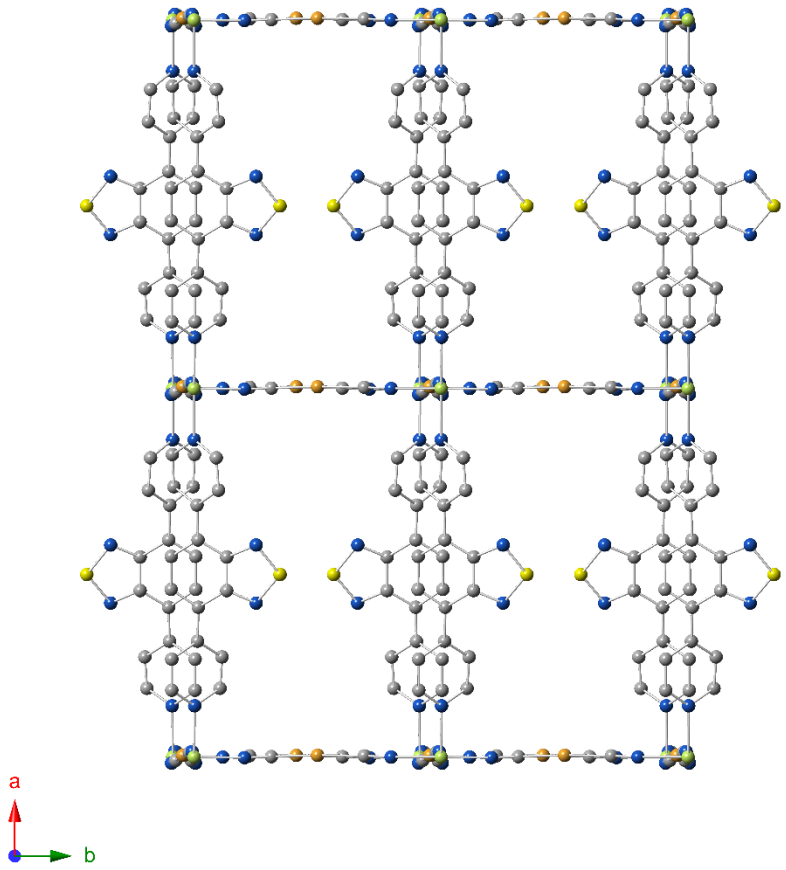

Fig. S3.0 Au ⊃ chry at 250 K viewed along the *c*-axis. Hydrogen atoms and guest molecules have been omitted for clarity. Atom colours: C (grey), N (blue), S (yellow), Fe (green), Au (gold).

Table S2.1 Crystallographic data for **Au ⊃ chry** at 250 K, 185 K, and 100 K.

	250 K	185 K	100 K
Empirical formula	$C_{32}H_{20.5}N_{9.5}SAu_2Fe$	$C_{32}H_{20.5}N_{9.5}SAu_2Fe$	$C_{32}H_{20.5}N_{9.5}SAu_2Fe$
Formula weight / g mol^{-1}	1019.92	1019.92	1019.92
Crystal system	Monoclinic	Monoclinic	Monoclinic
Space group	$P2_1/c$	$P2_1/c$	$P2_1/c$
Radiation / Å	0.71073 (Mo Kα)	0.71073 (Mo Kα)	0.71073 (Mo Kα)
***Z*(*Z'*)**	4(1)	4(1)	4(1)
***a* / Å**	15.8841(3)	15.619(3)	15.5337(6)
***b* / Å**	10.4933(2)	10.248(2)	10.1502(3)
***c* / Å**	20.8704(5)	20.432(4)	20.2438(6)
***β* / °**	99.856(2)	96.89(3)	96.294(3)
***V* / Å^3**	3427.27(12)	3246.9(12)	3172.60(17)
***F*(000)**	1916	1916	1916
Crystal size / mm^3	0.191 × 0.133 × 0.086	0.150 × 0.120 × 0.075	0.191 × 0.133 × 0.086
2θ range for data collection / °	3.248–25.027	1.131–30.569	3.315–29.308
Index ranges	-18 ≤ h ≤ 18, -12 ≤ k ≤ 12, -24 ≤ l ≤ 24	-21 ≤ h ≤ 22, -14 ≤ k ≤ 14, -29 ≤ l ≤ 29	-20 ≤ h ≤ 21, -13 ≤ k ≤ 12, -27 ≤ l ≤ 27
T_{min}, T_{max}	0.775, 1.000	0.2085, 0.2796	0.722, 1.000
Reflections collected	32778	173286	35570
R_{int}	0.0629	0.0548	0.0555
R_{sigma}	0.0553	0.0351	0.0565
ρ_{calc} **/ g cm^{-3}**	1.977	2.086	2.135
μ **/ mm^{-1}**	9.055	9.559	9.782
Data/restraints/parameters	6034/358/483	9971/449/458	7892/492/470
R_1 **[*I* > 2σ(*I*), all data][a]**	0.0432, 0.0727	0.0354, 0.0688	0.0483, 0.0736
wR_2 **[*I* > 2σ(*I*), all data][b]**	0.0979, 0.1094	0.0714, 0.0895	0.0955, 0.1047
Goodness-of-fit on F^2	1.096	1.225	1.121
$\Delta\rho_{max}$, $\Delta\rho_{min}$ **/ e Å^3**	2.7/-1.1	3.0/-2.2	3.6/-1.6
CCDC number	2166790	2166789	2166788

[a] $R_1 = \Sigma||F_o| - |Fc||/\Sigma|F_o|$. [b] $wR_2 = [\Sigma[w(F_o^2 - F_c^2)^2]/\Sigma[w(F_o^2)^2]]^{1/2}$.

Table S2.2 Selected bond lengths and angles of **Au ⊃ chry** at 250 K.

Bond length or angle	**Au ⊃ chry** (250 K)
<Fe1–N> / Å [a]	2.16
Au1–Au2 / Å	3.2742(6)
Σ(Fe1) / ° [b]	13.66(97)
C1–Au1–C3 / °	177.6(4)
C2–Au2–C4 / °	177.6(4)
S1–N7$_{benzothiadiazole}$ / Å	1.610(10)
S1–N8$_{benzothiadiazole}$ / Å	1.617(9)
N7–S1–N8$_{benzothiadiazole}$ / °	101.5(5)

[a] Average Fe-N bond length. [b] Octahedral distortion parameters calculated using the twelve *cis* N-Fe-N bond angles for octahedral Fe(II).[8]

Table S2.3 Selected bond lengths and angles of **Au ⊃ chry** at 100 K.

Bond length or angle	**Au ⊃ chry** (100 K)
<Fe1–N> / Å [a]	1.96
Au1–Au2 / Å	3.2434(5)
Σ(Fe1) / ° [b]	9.20(7)
C1–Au1–C3 / °	177.3(4)
C2–Au2–C4 / °	176.4(3)
S1–N7$_{benzothiadiazole}$ / Å	1.615(8)
S1–N8$_{benzothiadiazole}$ / Å	1.627(8)
N7–S1–N8$_{benzothiadiazole}$ / °	101.4(4)

[a] Average Fe-N bond length. [b] Octahedral distortion parameters calculated using the twelve *cis* N-Fe-N bond angles for octahedral Fe(II).[8]

S3 – Powder X-Ray Diffraction

Variable temperature powder X-ray diffraction (PXRD) patterns were measured on a STOE STADI P diffractometer operating in Debye-Scherrer geometry with monochromated Mo-K_α (λ = 0.70930 Å) radiation and three Mythen 1K strip detectors in stationary mode, covering a 2θ range of 0–55°. Temperature control was achieved using an Oxford Cryostreams nitrogen cryostream system. Diffraction patterns were collected in increments of 5 K with five minute exposure times between the range 100–300 K. Single crystals of **Au ⊃ chry** were first washed with freshly made ethanol:acetonitrile (1:1) and then ground to produce a bulk polycrystalline sample before being loaded as a solid suspension into a 0.5 mm glass capillary. Centrifugation was applied to concentrate the powder before the capillary was flame-sealed to prevent solvent loss.

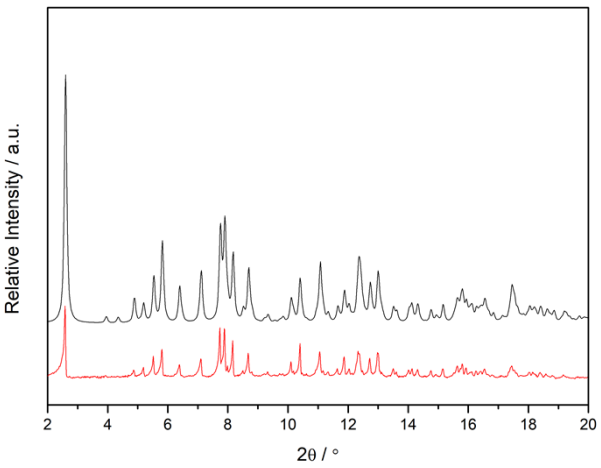

Fig. S3.1 Comparison of experimental (red) and calculated powder X-ray diffraction patterns (black) of **Au** ⊃ **chry** at 250 K.

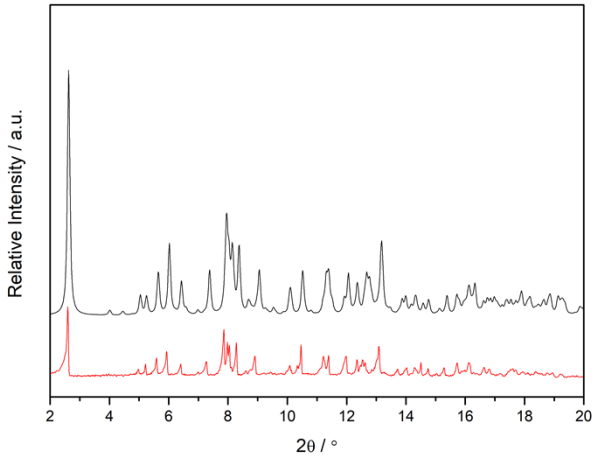

Fig. S3.2 Comparison of experimental (red) and calculated powder X-ray diffraction patterns (black) of **Au** ⊃ **chry** at 185 K.

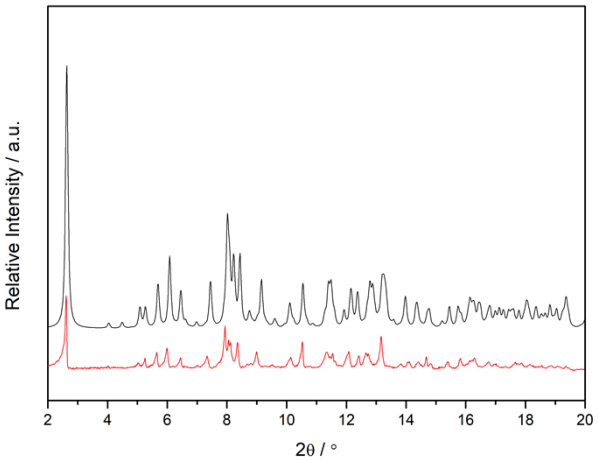

Fig. S3.3 Comparison of experimental (red) and calculated powder X-ray diffraction patterns (black) of **Au** ⊃ **chry** at 100 K.

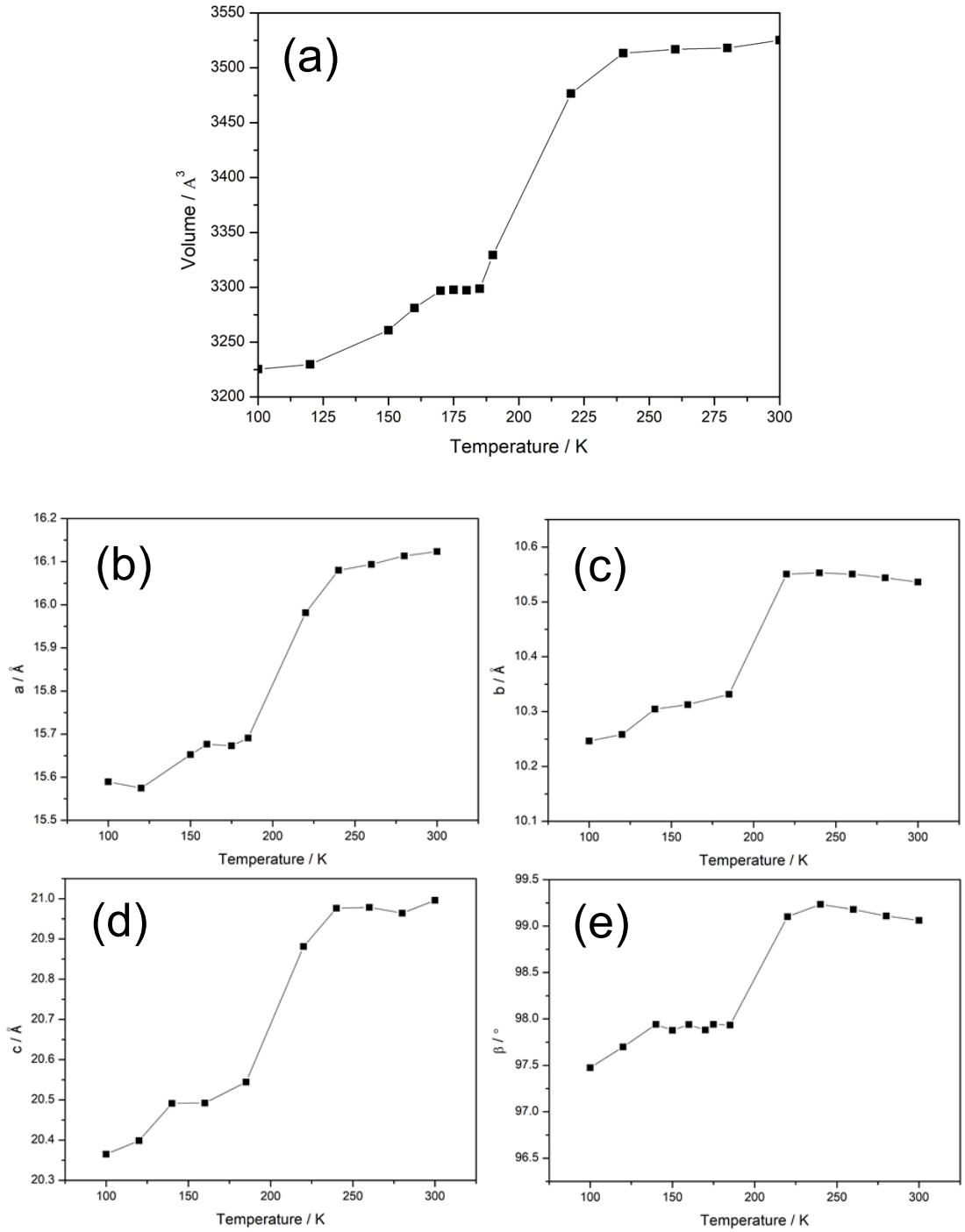

Fig. S3.4 Variable temperature Le Bail fit of **Au ⊃ chry** showing the change in cell parameters between the range 300–100 K. (a) volume, (b) *a*-axis, (c) *b*-axis, (d) *c*-axis, (e) β angle.

S4 – Magnetic susceptibility

Variable temperature magnetic susceptibility data were collected at The University of New South Wales, Sydney, Australia, on a Quantum Design VersaLab equipped with a vibrating sample magnetometer (VSM). Experiments were conducted under an applied magnetic field of 3000 Oe (0.3 T). Data were acquired in continuous sweep mode between 300–60 K at a scan rate of 2 K min^{-1}. Single crystals of **Au ⊃ chry** were washed in freshly made ethanol:acetonitrile (1:1), loaded into chemically resistant Swagelok perfluoroalkoxy alkane (PFA) tubing (0.125" OD x wall 0.030"), and then flame-sealed to prevent solvent loss. The PFA sample holder tubes were then placed into a brass half-tube before being attached to a VSM sample rod (appropriate for the small bore option) and measured.

S5 – Raman Spectroscopy

Raman scattering spectra were acquired using a Renishaw InVia Qontor confocal spectrometer. Samples were excited using a 50 mW diode green laser outputting an excitation wavelength of 532 nm (5% laser power) and were referenced internally with respect to Si at 520.5 ± 0.1 cm^{-1}. Polycrystalline chrysene was loaded into 0.5 mm glass capillaries and then flame-sealed before being placed on a Linkam FTIR 600 cryostage fitted with a glass window. A single crystal of **Au ⊃ chry** was alternatively placed directly from the crystallisation mother liquor onto the same cryostage. A Leica long 50× objective was used to focus the laser beam perpendicularly onto the sample. Spectra were recorded on a Renishaw Centrus 2957N7 CCD detector using ten second exposure times which were averaged over three accumulations. Data were processed (WiRE 5.0, Renishaw) with baseline subtractions and cosmic ray removal as required. The "waviness" of the background in Fig S5.2 is possibly due to laser-induced Raman fluorescence of chrysene or due to interference within the sample.

Raman spectroscopy confirmed the inclusion of chrysene in **Au⊃chry**. A single crystal of **Au⊃chry** was washed in a 1:1 mixture of ethanol and acetonitrile to remove any unincluded chrysene from the crystallisation mother liquor. The crystal was air dried before Raman spectra were acquired to ensure the absence of any surface acetonitrile generating a false positive in the spectrum. The most salient feature in the Raman spectrum of **Au⊃chry** is the ν(C≡N) symmetric stretch at 2189 cm^{-1} from the host framework. Peaks at 1551 cm^{-1} and 1612 cm^{-1} represent the ν(C=C) aromatic ring vibrations in the pillaring ligand. There is a weaker signal at 2249 cm^{-1} indicative of the ν(C≡N) stretch of included pore acetonitrile. Other vibrational bands observed at 1572 cm^{-1}, 1429 cm^{-1}, 1378 cm^{-1}, 1332 cm^{-1}, 1224 cm^{-1}, 1018 cm^{-1}, are consistent with previous literature reports of chrysene.[9]

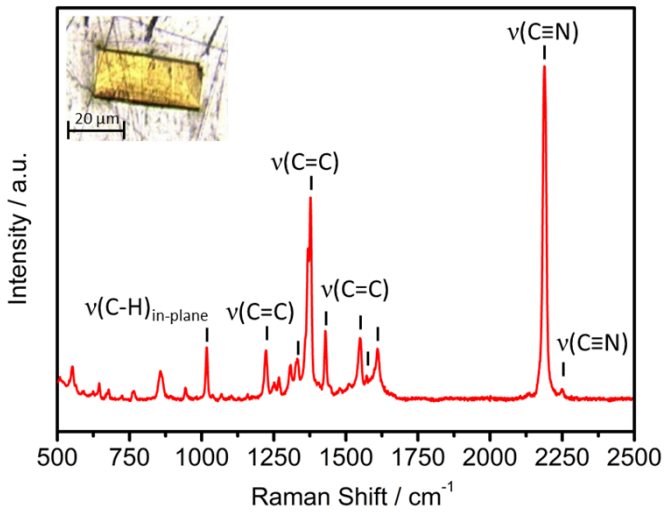

Fig. S5.1 Single crystal Raman spectrum of **Au ⊃ chry** with key Raman modes indicated (inset: crystal used).

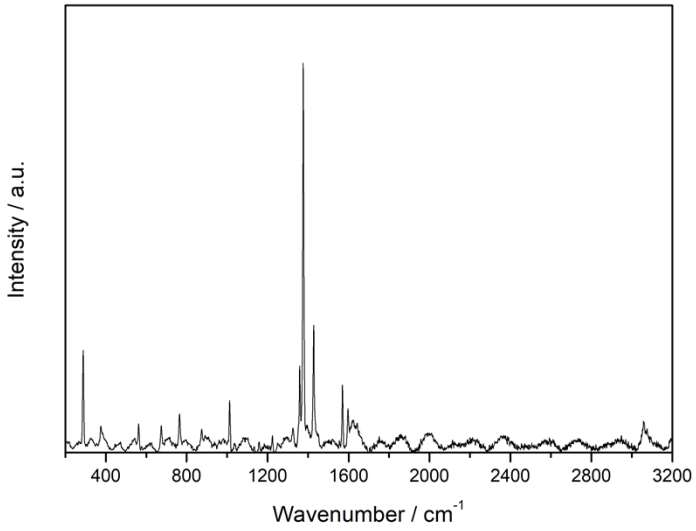

Fig. S5.2 Raman spectrum of powdered chrysene.

S6 – Thermogravimetric Analysis

Thermogravimetric analysis was performed on a TA Instruments Discovery TGA Thermogravimetric Analyser. Single crystals of **Au ⊃ chry** were loaded onto a platinum pan sample holder and then an isothermal heating step was performed at 50 °C for 20 minutes. Following removal of surface solvent, a ramping step was included to a final temperature of 650 °C at a rate of 10.00 °C min^{-1} and under a continuous stream of dry nitrogen (0.1 mL min^{-1}). Acetonitrile within the pores of **Au ⊃ chry** was not observed to occur with any mass loss across the range 50–300 °C and were likely lost gradually. Around 320 °C there is a slight mass loss before **Au ⊃ chry** decomposes in two-steps between the range 350–500 °C.

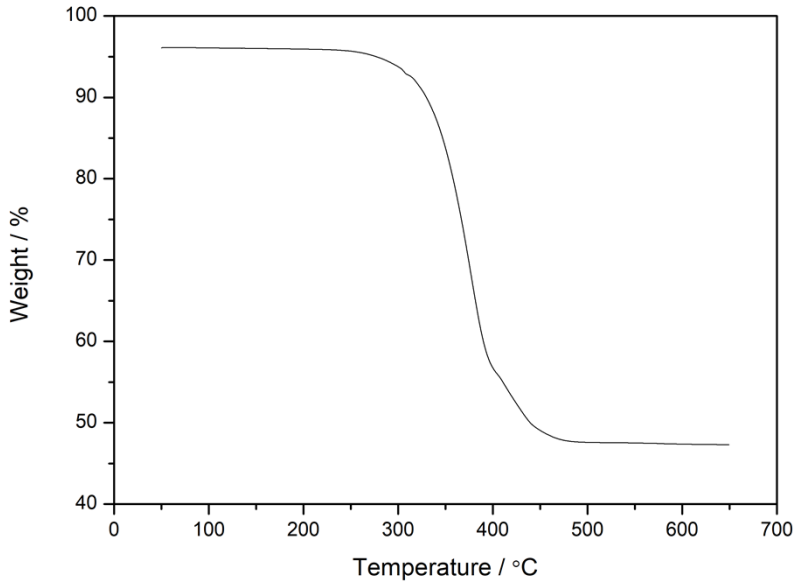

Fig. S6 TGA of **Au ⊃ chry** with heating from 50–650° at a rate of 10.0 °C min^{-1}. Isothermal step not shown.

S7 – UV-Visible Spectroscopy

Diffuse reflectance solid-state UV-Vis experiments were conducted on a Cary5000 UV-Vis-NIR spectrophotometer with a Praying Mantis attachment. Baseline spectra were acquired using $BaSO_4$ background. Powdered sample of **Au ⊃ chry** were loaded as a suspension in ethanol:acetonitrile (1:1) onto a flattened sample of $BaSO_4$ and were then allowed to air-dry before measurements. Scans were measured between the range 200–800 nm at 10 nm s^{-1}. Diffuse reflectance data presented in Kubelka-Munk units ($F(R) = (1-R)^2/2R$).

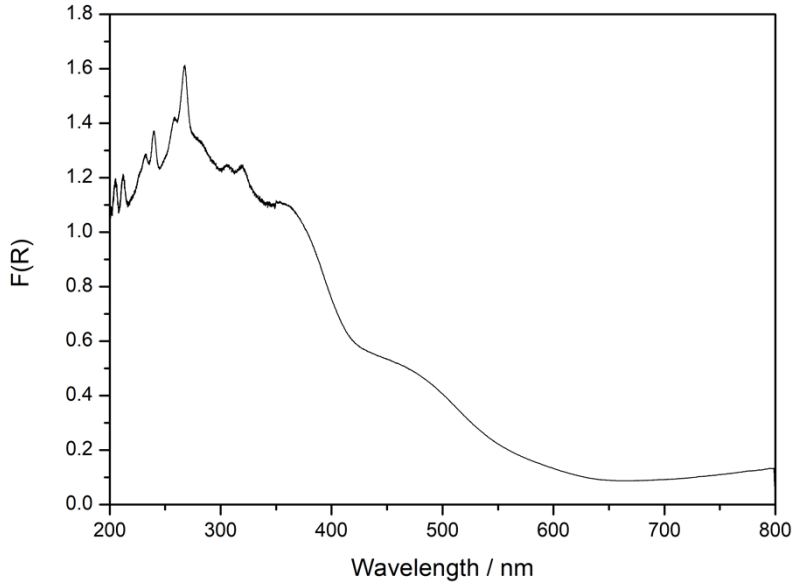

Fig. S7 UV-Vis spectrum of **Au ⊃ chry**. Peaks at 258 nm and 267 nm assigned to $\pi \rightarrow \pi^*$ transitions in included chrysene.[10]

S8 – Density Functional Theory

Density Functional Theory (DFT) calculations were performed for pairs of chrysene molecules to model the relative energies of different possible configurations within the pore structure. All calculations were performed in DMol3 v2017 within Materials Studio,[11,12] using the PBE[13] GGA functional and Grimme[14] dispersion correction with an overall "Fine" accuracy setting. A chrysene molecule was first geometry-optimised and the resulting geometry was used for subsequent calculations. Pairs of chrysene molecules were placed in the up-down and up-up arrangements (Fig. S8.1). In both calculations the molecules were co-planar and aligned parallel to each other. The calculated energy of the closer up-down interaction was 10 kJ mol^{-1} lower (more stable) than the more distant up-up interaction. Finally, a geometry optimisation was performed on an up-down pair of chrysene molecules constrained to be co-planar, which allowed the molecules the find their lowest-energy side-to-side configuration. Although a π-stacked arrangement would be more stable, the constraints of the pore environment in **Au ⊃ chry** do not allow stacking. This optimisation resulted in only small changes to the molecular arrangement and a further 5 kJ mol^{-1} energy reduction (for a total -15 kJ mol^{-1} relative to the up-up configuration). The optimised geometry remained very similar to the crystallographic up-down arrangement (Fig. S8.2).

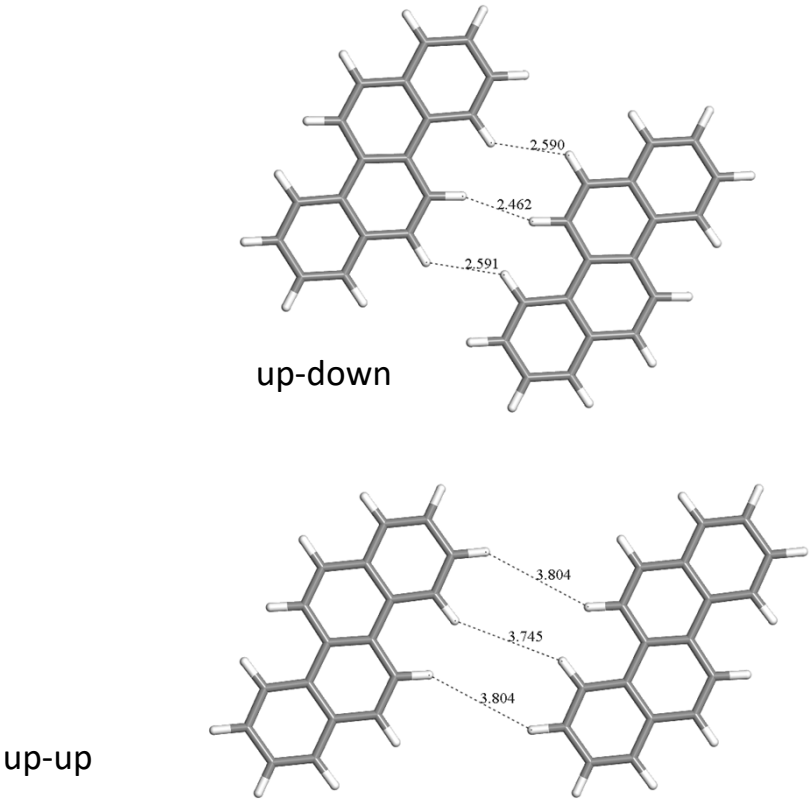

Fig. S8.1 Chrysene up-down (left) and up-up (right) pairs for which DFT energies were calculated. Labelled distances are in Å.

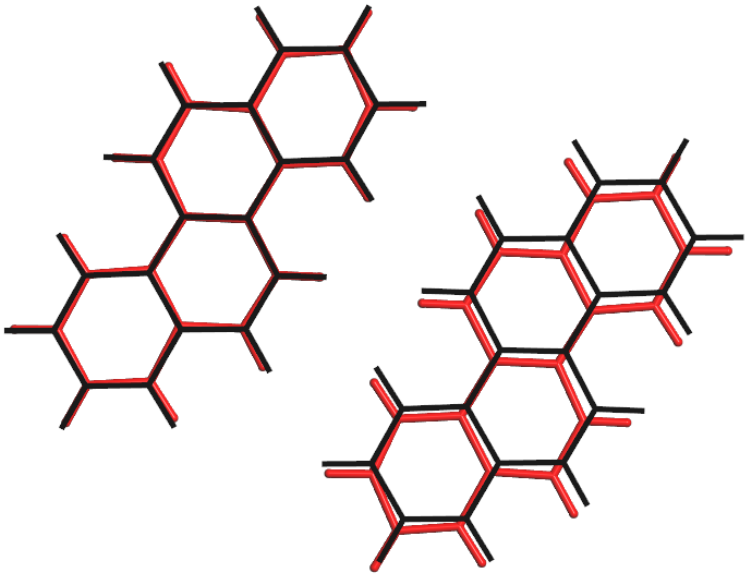

Fig. S8.2 DFT geometry-optimised configuration of a side-by-side chrysene pair (black) overlaid with the crystallographic up-down configuration (red). The similarity in the structures indicates that the crystallographic structure represents a stable arrangement of the molecules.

S9 – References

1. M. Akhtaruzzaman, M. Tomura, J.-I. Nishida and Y. Yamashita, *J. Org. Chem.*, 2004, **69**, 2953–2958.

2. Agilent (2014). *CrysAlis PRO*. Agilent Technologies Ltd, Yarnton, Oxfordshire, England.

3. Bruker (2012). *APEX2*, Bruker AXS Inc., Madison, Wisconsin, USA.

4. G. M. Sheldrick, *Acta Cryst. A*, 2015, **71**, 3–8.

5. G. M. Sheldrick, *Acta. Cryst. C*, 2015, **C71**, 3–8.

6. O. V. Dolomanov, L. J. Bourhis, R. J. Gildea, J. A. K. Howard and H. Puschmann, *J. Appl. Cryst.*, 2009, **42**, 339–341.

7. A. L. Spek, *Acta Cryst.* 2009, **D65**, 148–155.

8. M. A. Halcrow, *Chem. Soc. Rev.*, 2011, **40**, 4119–4142.

9. A. I. Alajtal, H. G. Edwards, M. A. Elbagerma and I. J. Scowen, *Spectrochim. Acta A*, 2010, **76**, 1–5.

10. G. M. Badger, N. C. Jamieson and G. E. Lewis, *Aust. J. Chem.*, 1965, **18**, 190–198.

11. B. Delley, *J. Chem. Phys*. 1990, **92**, 508–517.

12. B. Delley, *J. Chem. Phys*. 2000, **113**, 7756–7764.

13. J. P. Perdew, K. Burke and M. Ernzerhof, *Phys. Rev. Lett.*, 1996, **77**, 3865–3868.

14. S. Grimme, *J. Comput. Chem.* 2006, **27**, 1787–1799.